Liquid Crystals
Publication details, including instructions for authors and subscription information:
http://www.informaworld.com/smpp/title~content=t713926090

X-ray reflectivity from insoluble monolayers spread on aqueous subphases

R. M. Richardson[a]; S. J. Roser[a]
[a] University of Bristol, School of Chemistry, Cantock's Close, Bristol, England

To cite this Article Richardson, R. M. and Roser, S. J.(1987) 'X-ray reflectivity from insoluble monolayers spread on aqueous subphases', Liquid Crystals, 2: 6, 797 — 814
To link to this Article: DOI: 10.1080/02678298708086336
URL: http://dx.doi.org/10.1080/02678298708086336

LIQUID CRYSTALS, 1987, VOL. 2, NO. 6, 797–814

X-ray reflectivity from insoluble monolayers spread on aqueous subphases

by R. M. RICHARDSON and S. J. ROSER
University of Bristol, School of Chemistry, Cantock's Close, Bristol BS8 1TS, England

(*Received 22 April 1987; accepted 11 July 1987*)

The technique of X-ray reflection is used to study the structure of an insoluble monolayer spread on an aqueous subphase. The feasibility of the technique as a non-invasive structural probe for liquid surfaces is demonstrated. A comparison of the X-ray reflectivity from docosanoic acid spread on $2{\cdot}5 \times 10^{-4}$ molar solutions of caesium chloride, cadmium chloride and lanthanum chloride shows that practically all of the cadmium and lanthanium ions are within 15 Å of the acid head groups whereas there is no evidence for such binding with caesium. The pH dependence of the amount of bound cadmium is used to show that a pK value of $5{\cdot}35 \pm 0{\cdot}05$ describes the conversion from acid to cadmium soap.

1. Introduction

There is currently much interest in the properties of insoluble monolayers at the water/air interface because they can be deposited on a solid substrate using the Langmuir–Blodgett (LB) technique. This offers the possibility of controlling the composition and structure of a film at a molecular level and has considerable potential for the fabrication of electronic or optic devices [1]. If this potential is to be developed so that molecules with useful electrical or optical properties can be reliably incorporated into LB films, it is important that the deposition process is well understood. A prerequisite for this is that the nature of the spread monolayer must also be well understood. Surface properties such as surface pressure, surface potential and surface rheology have been used for many years to study spread monolayers (see, e.g., [2]), but none is capable of giving direct structural information. In this paper we report the use of X-ray reflectometry to study the structure of a spread monolayer. Initial results are presented on a saturated, long chain carboxylic acid, which has already been studied by several other techniques, in order to demonstrate the feasibility of the X-ray reflectivity technique as a means of obtaining structural information in a direction perpendicular to the liquid/air interface.

2. Introduction to the X-ray reflection technique

The reflection of monochromic X-rays from pure liquid or liquid crystal surfaces has been demonstrated using radiation from synchrotron or rotating anode sources [3, 4]. Below the critical angle, θ_c, virtually all the incident X-ray intensity is externally reflected by the liquid so the reflectivity is close to unity. Above θ_c, as the glancing angle of incidence, θ, is increased, the reflectivity falls off rapidly and reaches a value of typically 10^{-6} by $\theta/\lambda \sim 0{\cdot}025\,\text{Å}^{-1}$. The detail in the dependence of the reflectivity on angle of incidence contains information on the structure of the air/liquid interface in a direction normal to the surface and this is exploited in the work presented here.

Section 2.1 gives a resumé of the relationship between the X-ray reflectivity and the surface structure. Section 3.1 describes the apparatus that was used to make reflectivity measurements on spread monolayers and the results are presented in § 4 and discussed in § 5.

2.1. *Resumé of X-ray reflectivity theory*

There are several approaches to the calculation of the X-ray (or neutron) reflectivity profile from macroscopic surfaces. Some previous work [5, 6] has used an analogue of the method used for calculating the reflectivity of multiple strata for visible light [7]. This method of calculation would seem to be free from any serious approximations for neutron or X-ray reflectivity calculations and we shall regard it as 'correct'. Its disadvantage is that it becomes rather cumbersome if there are diffuse interfaces between different strata, and it is not easy to see a simple relationship between the structure and the reflectivity. There are two approximate approaches [3, 8] to the calculation and we have used the one introduced by Als Nielsen (see [3] and references cited within) since it gives a reasonable approximation to the 'correct' calculation (i.e. within 1 per cent for the sample studied in this work over the entire scattering angle range). We have also verified numerically that for the system studied here, absorption of radiation can be neglected without introducing any significant error. This approximate theory is summarized and applied to interfaces with the absorbed film in the following paragraph in order to provide a basis for a qualitative and quantitative understanding of the reflectivity measurements presented here.

We consider an interface between two bulk phases with an absorbed thin film. The scattering length density (proportional to the electron density for X-ray scattering) of such a system is represented in figure 1 (*a*). The reflectivity as a function of the glancing angle, θ, is given to a good approximation [3] by the formula

$$R(\theta) = R_F(\theta)|\phi(Q)|^2, \tag{1}$$

where $R_F(\theta)$ is the reflectivity that would be given by an ideally sharp interface with no adsorbed film. It can be calculated using the Fresnel reflectivity formula ([7] and Appendix) and we will refer to it as the Fresnel factor. The second factor on the right-hand side of the equation is the modulus squared of the Fourier transform of the scattering density gradient

$$|\phi(Q)|^2 = \left|\frac{1}{\varrho_s - \varrho_a}\int_{-\infty}^{\infty}\left(\frac{\partial\varrho(z)}{\partial z}\right)\exp(iQz)\,dz\right|^2, \tag{2}$$

where

$$Q = \frac{4\pi}{\lambda}\left\{\left[\left(\frac{\mu_f}{\mu_a}\right)^2 - 1\right] + \sin^2\theta\right\}^{1/2} \tag{3}$$

above the critical angle and $Q = 0$ below it. λ is the wavelength of radiation used and $\mu_f(\mu_a)$ the refractive index of the film (or air). At angles significantly above the critical angle $Q \approx (4\pi\sin\theta)/\lambda$. The refractive index is related to the electron density by

$$\mu = 1 - \frac{\lambda^2}{2\pi}Nar_e, \tag{4}$$

where N is the number of molecules per unit volume, a is the number of electrons per molecule and r_e is the scattering length of an electron ($2{\cdot}85 \times 10^{-5}$ Å). $|\phi(Q)|^2$ depends upon the structure of the interface and we shall refer to it as the film factor.

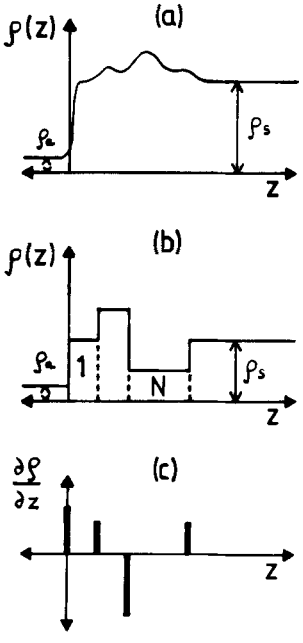

Figure 1. Schematic profiles of scattering density, $\varrho(z)$ and its derivative.

It is particularly useful since it is easy to calculate and describes the scattering in the usual kinematic approximation which is used in conventional diffraction experiments.

If the film can be described as a series of M sharp strata as shown in figure 1 (b), then $[d\varrho(z)]/(dz)$ is a series of delta functions (as shown in figure 1 (c))

$$\frac{d\varrho(z)}{dz} = \sum_{j=0}^{M} (\varrho_{j+1} - \varrho_j)\,\delta(z - z_j), \tag{5}$$

where ϱ_j is the scattering density in stratum j (with $0 \equiv a$ so $\varrho_0 = \varrho_a$ and $N + 1 \equiv s$ so $\varrho_{N+1} = \varrho_s$) and z_j is the distance of the strata $j/(j+1)$ interface from the surface. If the interfaces between the different strata are not sharp but have an error function scattering density profile, then the gradient becomes a series of gaussians,

$$\frac{d\varrho}{dz} = \sum_{j=0}^{M} (\varrho_{j+1} - \varrho_j)\,g(z - z_j, u_j), \tag{6}$$

where

$$g(x, \sigma) = \frac{1}{\sqrt{(2\pi)}\,\sigma} \exp[-x^2/(2\sigma^2)], \tag{7}$$

so u_j defines the sharpness of the strata $j/(j+1)$ interface. Using the standard result for the Fourier transform of a gaussian we obtain

$$|\phi(Q)|^2 = \frac{1}{(\varrho_s - \varrho_a)^2} \left| \sum_{j=0}^{M} (\varrho_{j+1} - \varrho_j) \exp(iQz_j - \tfrac{1}{2}Q^2u_j^2) \right|^2. \tag{8}$$

It can be seen that a large value of u will cause $|\phi|^2$ to be severely reduced at large Q in a similar fashion to the effect of the temperature factor used in conventional crystallography. Substituting equations (A 1) and (8) into equation (1) gives a useful formula for the calculations of reflectivity profiles; it could easily be adapted to other functional forms of $\varrho(z)$.

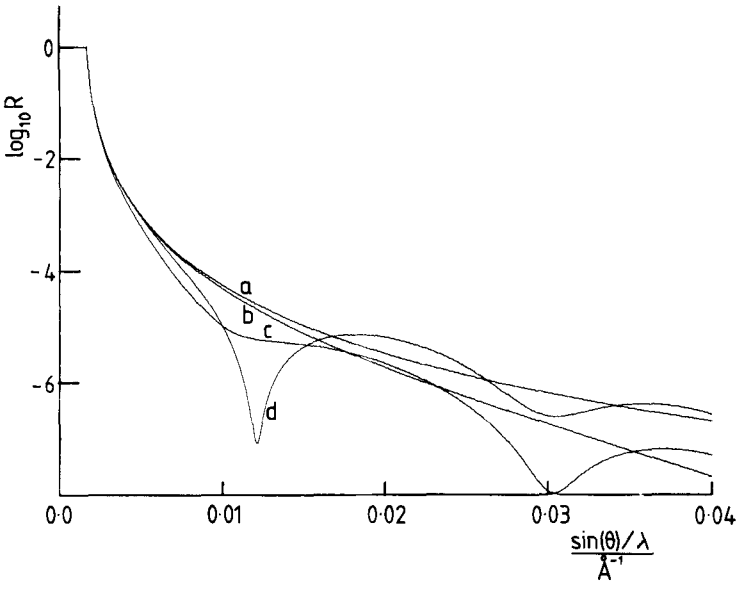

Figure 2. X-ray reflectivity, R, as a function of $\sin\theta/\lambda$ for simple models of the interface.

The film factor, $|\phi(Q)|^2$, contains all of the information on the structure of the adsorbed film. The film factor may in general cause R to have positive or negative deviations from R_F depending upon the structure of the interfacial region. It is useful to consider how $|\phi|^2$ behaves for the special case of only one stratum ($M = 1$) of thickness d. It can be shown from equation (8) that if $\varrho_a < \varrho_l < \varrho_s$, then $|\phi|^2$ will be a minimum when

$$(n - \tfrac{1}{2})\lambda = 2d \sin\theta, \tag{9}$$

where $n = 1, 2, 3$, etc. and inspection of equation (8) shows that $|\phi|^2$ can only cause negative deviations from R_F. If $\varrho_a < \varrho_f > \varrho_s$ then $|\phi|^2$ will be a minimum when

$$n\lambda = 2d \sin\theta, \tag{10}$$

where $n = 1, 2, 3$, etc. and inspection of equation (8) shows that $|\phi|^2$ can only cause positive derivations from R_F. Figure 2 illustrates the form of the reflectivity curve for some simple models. It shows the reflectivity for (*a*) an ideal air/water interface, (*b*) an air/water interface with an error function density profile ($\sigma = 3{\cdot}0$ Å) and (*c*) an air/water interface with a 20 Å film with 80 per cent of the electron density of water, and (*d*) shows the effect of a sublayer of high electron density below the film. If there is more than one stratum in the adsorbed film, no such simple formulae exist and equation (8) must be used to interpret the data.

The strategy that we have used to analyse the data in this network is discussed in § 4.2.

3. Experimental

3.1. *X-ray reflectometer*

The X-ray reflectometer was based on a design by Bowler *et al.* which will be published in detail elsewhere [9]. It was supplied by Ursar Scientific Instruments,

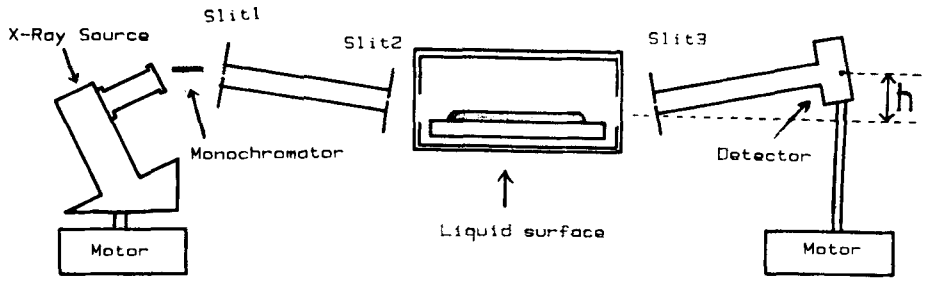

Figure 3. Schematic diagram of the X-ray reflectometer.

Oxford, and later modified in the Mechanical Workshop, School of Chemistry, Bristol. Data acquisition software was written by one of us (SJR). The important feature of the X-ray reflectometer is that the source and detector can both move simultaneously in the vertical plane thus allowing the surface of the sample to remain level during a theta-two theta scan. The source is a conventional sealed 1·5 kW X-ray tube with a copper anode and it was generally run at 40 kV and 30 mA. A current and voltage stabilized generator (0·03 per cent for 10 per cent mains fluctuation) is used so that intensities from different runs can be reliably intercompared. Both the source and the detector are at 0·55 m from the sample position and the ribbon beam is collimated by slits defined by tantalum rods at 0·1 m (0·2 mm) and 0·45 m (0·5 mm) from the sample, as shown in figure 3. The detector arm also had a 0·5 mm slit at 0·1 m from the sample. The K_α component of the radiation (wavelength, $\lambda = 1{\cdot}54$ Å) was selected by a nickel filter and a 0·4° mosaic spread graphite monochromator. The heights, h, in figure 3 of the source and detector arms were controlled by stepping motors from a BBC microcomputer and measuring using an optical linear displacement transducer (Mitutoyo). In the experiments reported here, the arm heights were stepped in units of 0·2 mm from 0 to 35 mm giving 176 angular steps of 0·36 mrad. With the slit widths used, an angular beam divergence of 1·0 mrad is expected. A flux of about 10^7 counts per second was obtained at the sample position. The minimum reflectivity that can be successfully measured depends upon the background from the diffuse scattering by the sample and from air scattering. In practice we found that reflectivities of less than 10^{-6} were measurable. For this work, a counting time of 15 s at each angle was used and the total time for a scan was $1\frac{1}{4}$ h. At angles below 5 mrad the beam was attenuated to avoid dead time errors from the detector. The counts versus angle data were acquired by the BBC microcomputer and transferred to a VAX computer for further analysis.

3.2. *Langmuir trough*

The spread monolayers were prepared on a small (150 × 90 × 30 mm) glass Langmuir trough. This was contained in a hermetically sealed perspex box with mylar windows for the extrance and exist of the X-ray beam. This box kept the level of the liquid, and hence the zero angle, constant for at least 2 days. The box was supported from the floor independently from the rest of the spectrometer in order to avoid transmitting vibrations to the liquid sample and, probably because the laboratory floor was in contact with bed rock, vibrations of the liquid surface did

not prove to be troublesome. A mechanical vertical adjustment was placed between the perspex box and the pillar supporting it so that the liquid could be brought to the correct height by halving the straight through intensity with the arms level. Levelling screws were also provided so that the top edge of the trough could be levelled.

The surface area of the insoluble monolayer was controlled by manually operated teflon booms running on the flat ground edge of the trough. This edge was rendered hydrophobic by treatment with dimethyldichlorsilane solution so that the meniscus could be about 2 mm clear of the edge. The surface pressure was measured by a filter paper Wilhelmy plate with a Gould Statham force transducer and the pH of the subphase was measured using a glass electrode. All measurements were done at a room temperature of 22°C.

3.3. *Materials and film preparation*

The trough and associated hardware were cleaned using chloroform and then isopropyl alcohol before use and filled with water from a Millipore MilliQ system. The monolayer of docosanoic acid (ICN) was spread from a $1{\cdot}5 \times 10^{-3}$ molar solution in Aristar chloroform (BDH Chemicals Ltd.) which was allowed to evaporate before adjusting the surface pressure using the booms and closing the sealed box. The pH of the subphase was adjusted using Aristar hydrochloric acid or sodium hydroxide and the appropriate metal chloride was added to give a $2{\cdot}5 \times 10^{-4}$ molar solution.

The effects of divalent ions and subphase pH on the surface pressure–surface area isotherms for saturated carboxylic acid are now well known [10]. Figure 4 shows the effect of changing the pH of a subphase containing $2{\cdot}5 \times 10^{-4}$ M cadmium chloride. Univalent ions such as caesium have no such dramatic effect. At a surface pressure of 40 mN m^{-1} the acid molecules in the monolayer are believed to be perpendicular to the surface and close packed since they occupy an area of 21 Å^2 molecule^{-1}. In this work we have made a series of X-ray reflectivity measurements on docosanoic acid spread on dilute cadmium chloride solution as well as single measurements using caesium chloride and lanthanum chloride subphases. These ions were chosen

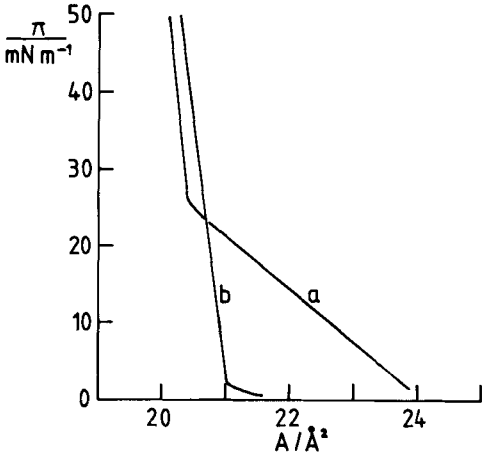

Figure 4. The schematic dependence of the surface pressure, π, on the area per molecule, A, at constant temperature for docosanoic acid, at pH values of (*a*) 5·2 and (*b*) 5·8 on $2{\cdot}5 \times 10^{-4}$ M cadmium chloride.

because (like cadmium) they are not hydrolyzed in aqueous solution at a pH of 7 or less.

4. Results

The X-ray reflectivity profile of a pure water/air interface is shown in figure 7. The critical angle is visible although the critical edge is rather rounded. Above the critical angle the data show a smooth monotonic decay as expected from theory and as observed previously using synchroton radiation. Figure 5 shows the X-ray reflectivity profile for docosanoic acid on a subphase containing $2{\cdot}5 \times 10^{-4}$M cadmium chloride as a function of pH. It can be seen that there is a dramatic change in the profile in the pH range 4·5 to 6. The Debye screening length for the subphase is of the order of 100 Å so any diffuse atmosphere of cadmium ions would only affect the reflectivity data at very low angles. (At $\sin\theta/\lambda > 0{\cdot}04$ Å the contribution to the film factor for an exponential decay of characteristic length 100 Å is less than 5 per cent of its value at zero angle). We believe therefore that the changes in the reflectivity at $\sin\theta/\lambda \approx 0{\cdot}01$ Å^{-1} result from the adsorption of a Stern layer of cadmium ions in close association with the ionized head groups of the acid monolayer.

Figure 6 shows the reflectivity profiles (divided by the reflectivity expected from an ideal clean interface) for docosanoic acid on subphases containing approximately

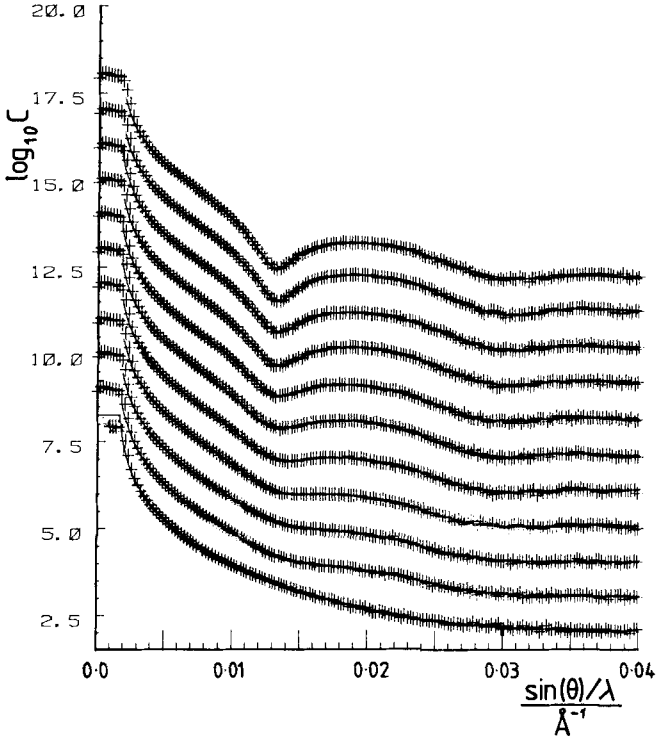

Figure 5. The points represent the X-ray counts C measured by reflection from a liquid/air interface. The line is a fit of equations (1) and (8) to the measured data. The lowest data set is from pure water. The other data sets have each been shifted by 10 for clarity and represent reflected X-ray counts from docosanoic acid on $2{\cdot}5 \times 10^{-4}$M cadmium chloride at pH values of (from bottom to top) 2·75, 4·0, 4·5, 5·25, 5·5, 5·75, 6·0, 6·25, 6·5 and 7·0.

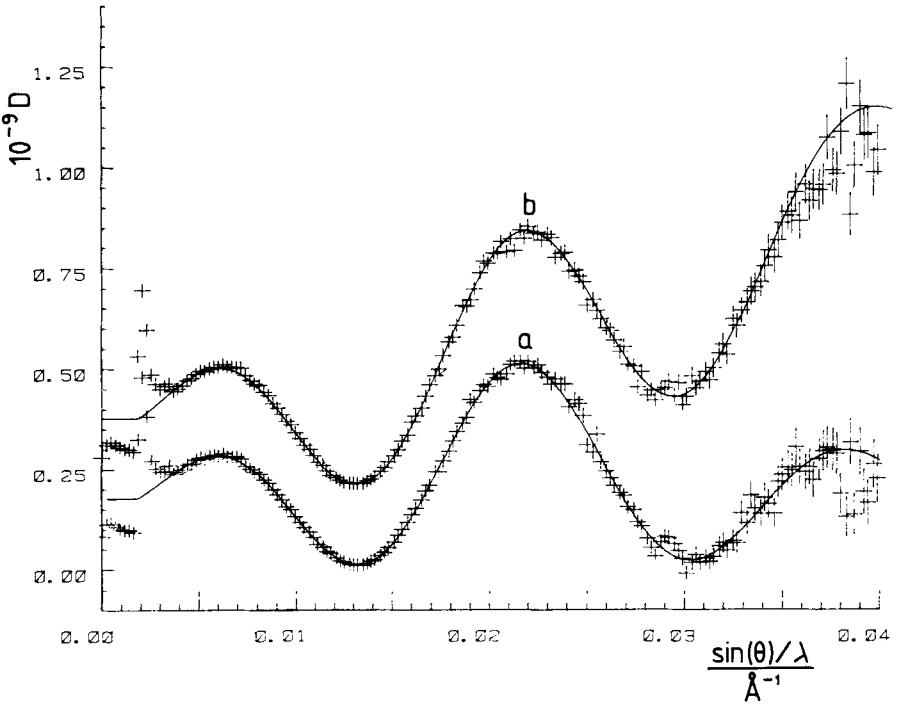

Figure 6. The reflected X-ray counts divided by the Fresnel factor, D, for a docosanoic acid monolayer with a subphase (pH = 6·5) containing (*a*) cadmium and (*b*) lanthanum.

2×10^{-4}M cadmium chloride and lanthanum chloride all at pH $\approx$6·5. On a substrate of approximately 2×10^{4}M caesium chloride at pH $\approx$6·5 the reflectivity profile was qualitatively different in that it was identical to that observed at pH of 2·75 (as shown in figure 5, second data set from bottom) where the ionization of the acid head group is suppressed. This demonstrates that few or none of the caesium ions are bound in a Stern layer while a significant proportion of the cadmium and lanthanum ions are bound to the ionized head groups. The reflectivity profiles are analysed in more detail in the following sections.

4.1. *Strategy for analysing the reflectivity profile from spread monolayers*

In principle it should be possible [8] to invert the reflectivity profile to obtain a scattering density profile. However, at this stage of the development of the X-ray reflectivity we believe it is safer to analyse the data by fitting reflectivity profiles for model scattering density profiles to the data. This allows resolution effects to be taken into account and avoids artifacts due to the finite angular range covered by the data. A computer program, FITLAY, based on the Harwell subroutine VA05A [11] has been written to fit equation (1) with $|\phi|^2$, as defined in equation (8), to the observed reflectivity data. The fitting was done by minimizing χ^2 where χ^2 is defined by the summation over the P data points

$$\chi^2 = \sum_{k=1}^{P} \left(\frac{c(\text{obs})_k - c(\text{calc})_k}{c(\text{err})_k} \right)^2, \tag{11}$$

where c_{calc} is derived from equation (1).

$$c(\text{calc})_k = c(\theta_k)S + B, \tag{12}$$

where S is a scaling parameter and B is a flat background. $c(\text{obs})_k$ is the number of counts in the detector at angle θ_k and $c(\text{err})_k$ is the square root of that number. Any of the model parameters (ϱ_j, d_j, u_j in equation (8)) could be fixed or allowed to vary when determining the fit.

Since the angular range and quality of our data impose a limit on the amount of information that can be extracted, we have attempted to find the simplest possible model that would give a satisfactory fit to the data. A model of one stratum on the subphase could be eliminated immediately because the position of the minima did not conform to those predicted by equations (9) or (10). Furthermore, the single stratum model is not able to predict the observation that the reflectivity from the spread monolayer is actually higher than that from an air/pure water interface around $\sin\theta/\lambda \approx 0{\cdot}02\,\text{Å}^{-1}$. The next degree of complexity involved two strata of different scattering densities on the subphase. One of these would represent the hydrocarbon chain layer and the other would represent a layer comprising water and cations associated with the carboxylic acid head groups. On grounds of relative electron density, we expect the carboxylic acid head groups to be represented as part of the second stratum and this is in fact borne out by the numerical results. Fitting this simple two strata model to the data involves the adjustment of eleven parameters, shown in table 1. The scattering density, ϱ, for the bulk phases and the close packed hydrocarbon chains can be calculated quite accurately from number density N of the molecules, the number of electrons per molecule, a, and the classical scattering length of an electron, r_e ($=2{\cdot}85 \times 10^{-5}$ Å), so two of the parameters can be fixed,

$$\varrho = Nar_e. \tag{13}$$

The scaling parameter depends on the incident intensity on the liquid surface, and since this was the same for all the reflectivity curves measured, it was determined by fitting a model representing equation (1) with no adsorbed film (i.e. $M = 0$ in equation (8)) to the reflectivity curve from a clean water surface. The region of the

Table 1. Parameters used in the two strata model for spread monolayers.

Stratum	Parameter	Value
Air	ϱ(air)	Fixed at $0{\cdot}0\,\text{Å}^{-2}$
	u(air/hydrocarbon)	Variable
Hydrocarbon stratum	ϱ(hydrocarbon)	Variable but $\sim 0{\cdot}9 \times 10^{-5}\,\text{Å}^{-2}$ expected
	d(hydrocarbon)	Variable but < 24 Å expected
	u(hydrocarbon/Cd + COO)	Variable
Cadmium stratum	ϱ(Cd + COO)	Variable
	d(Cd + COO)	Variable
	u(Cd + COO/water)	Variable
Subphase	ϱ(water)	Fixed at $0{\cdot}94 \times 10^{-5}\,\text{Å}^{-2}$
—	Scale factor	Fixed at $1{\cdot}78 \times 10^8$ counts by fit to clean water
—	Flat background	Variable but expect ~ 100 counts per 15 s

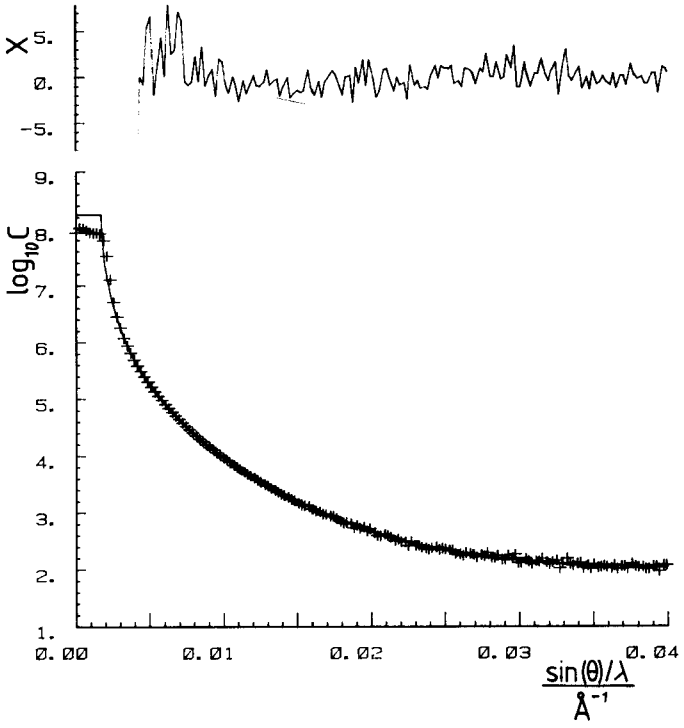

Figure 7. The points represent X-ray counts, C, measured by reflection from a pure water surface. The line through the points represents a model fit to the data and the upper graph is the weighted deviation between model and the data as used in equation (11).

Table 2. Parameters used to model the clean water surface.

Parameter	Value
ϱ(air)	Fixed at 0·0 Å^{-2}
u(air/water)	2·9 Å
ϱ(water)	Fixed at 0·94 × 10^{-5} Å^{-2}
Scale factor	1·78 × 10^{8} counts
Flat background	108 ± 3 counts per 15 s

curve below $\sin\theta/\lambda = 0{\cdot}004$ Å^{-1} was not fitted because the reflectivity curve is modified by instrumental resolution effects and any ripples on the surface, as can be seen in figure 7. The parameters in the model and the values determined by the fit are shown in table 2. The value for the scaling parameter was used as a fixed parameter for the rest of the fit. The value of u(air/water) of 2·9 Å compares well with the value of 3·2 Å given by measurements using synchroton radiation sources [3]. Figure 7 also shows a plot of (c(obs) − c(calc))/c(err) versus $\sin\theta/\lambda$. It can be seen that except at low angles where the data is statistically very accurate, the deviations lie between twice the expected error. At low angles a systematic error is apparent because of the very high statistical accuracy of the data. This is probably due to some surface ripples or lack of perfect alignment of the reflectometer.

The reflectivity data from the spread monolayers were therefore analysed using FITLAY by fitting equation (1) to the data using the parameters defined in table 1. The region in the data around and below the critical angle is modified by instrumental

resolution and surface ripple effects and so data at $\sin\theta/\lambda < 0{\cdot}004\,\text{Å}^{-1}$ were not included in the fit since, once the scaling factor is determined, very little structural information can be obtained from this region. It was found that including resolution and ripple effects made no significant difference to the best fit parameters determined by fitting at $\sin\theta/\lambda > 0{\cdot}004\,\text{Å}^{-1}$. Determining the best fit to the data was done in several stages with more parameters allowed to vary at each stage. Eventually the eight parameters indicated in table 1 were allowed to vary simultaneously in order to find the best fit of the model to the data.

4.2. *Numerical results*

The results of the eight-parameter fits to the data from docosanoic acid with cadmium ions in the subphase are given in table 3; the quality of the fits are shown by the lines in figure 5. Figure 8 shows the same fits but with the observed data (minus a flat background) divided through by $R_F(\theta)$ so that the fits display the observed and calculated film factor. This is quite a critical way of examining the quality of the fit since it emphasizes (visually) the low reflectivity parts. Figure 9 shows the scattering density profiles corresponding to the best fit parameters for some of the pH values.

It was found that there was some correlation between the parameters which describe the cadmium rich layer. The effect was analysed in some detail for the data at a pH of 6·25. The quality of fit did not deteriorate appreciably if the thickness of this layer was fixed at up to ± 3 Å from the best fit value of 9 Å. If it was fixed at less than 6 Å, the quality of the fit was satisfactory but the values of other parameters became

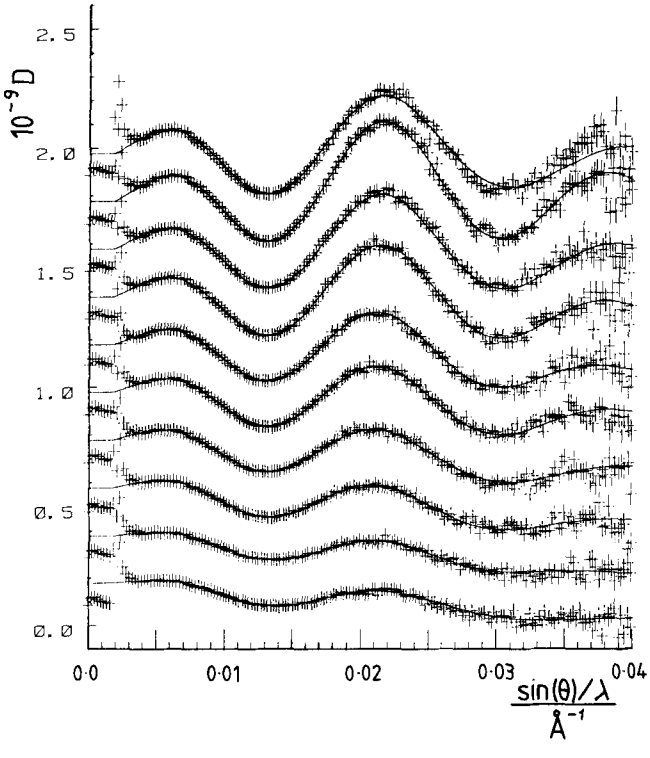

Figure 8. The reflected X-ray counts divided by the Fresnel factor, D, for the data in figure 5.

Table 3. Results from least square fitting.

Subphase salt	pH	u/Å air/hydrocarbon	$10^5\varrho$/Å^{-2} hydrocarbon	d/Å hydrocarbon	u/Å hydrocarbon Cd + COO	$10^5\varrho$/Å^{-2} Cd + COO	d/Å Cd + COO	u/Å Cd + COO/water	Background counts
$2{\cdot}5 \times 10^{-4}$M $CdCl_2$	2·75	2·9 ± 0·2	0·91 ± 0·01	23·0 ± 0·5	2·3 ± 1·9	1·08 ± 0·02	8 ± 2	5·2 ± 0·5	109 ± 4
	4·0	2·8 ± 0·1	0·94 ± 0·01	23·2 ± 0·7	0·0 ± 0·1	1·07 ± 0·02	11 ± 2	4·6 ± 1·3	108 ± 3
	4·5	3·0 ± 0·1	0·91 ± 0·01	22·3 ± 0·6	0·1 ± 0·3	1·04 ± 0·01	13 ± 2	5·0 ± 0·2	108 ± 3
	5·0	3·3 ± 0·1	0·93 ± 0·01	24·3 ± 0·7	0·0 ± 0·0	1·15 ± 0·01	9 ± 3	3·5 ± 0·5	113 ± 3
	5·25	3·2 ± 0·2	0·93 ± 0·01	24·4 ± 0·6	0·0 ± 0·02	1·24 ± 0·13	8 ± 4	4·7 ± 1·5	117 ± 4
	5·5	3·1 ± 0·1	0·93 ± 0·01	24·8 ± 0·2	0·0 ± 0·1	1·28 ± 0·01	8·2 ± 0·4	3·1 ± 0·3	112 ± 2
	5·75	3·0 ± 0·2	0·92 ± 0·01	24·1 ± 0·8	0·1 ± 0·2	1·25 ± 0·04	10 ± 2	2·0 ± 0·3	126 ± 8
	6·0	2·8 ± 0·3	0·92 ± 0·01	24·9 ± 1·0	1·0 ± 0·7	1·41 ± 0·14	8 ± 3	2·8 ± 0·7	131 ± 13
	6·25	2·9 ± 0·1	0·93 ± 0·01	24·9 ± 0·3	3·7 ± 0·8	1·48 ± 0·04	6·9 ± 0·6	3·5 ± 0·3	127 ± 6
	6·5	2·6 ± 0·1	0·94 ± 0·02	25·1 ± 1·2	1 ± 6	1·51 ± 0·23	7 ± 3	2·3 ± 0·9	126 ± 27
	7·0	3·3 ± 0·5	0·93 ± 0·03	24·4 ± 0·5	0·0 ± 0·01	1·67 ± 0·38	6 ± 4	4·8 ± 0·8	130 ± 32
$2{\cdot}5 \times 10^{-4}$M $LaCl_3$	6·5	3·3 ± 0·1	1·00 ± 0·01	25·8 ± 0·2	0·3 ± 1·1	3·24 ± 0·56	1·7 ± 0·2	3·5 ± 0·2	6 ± 3

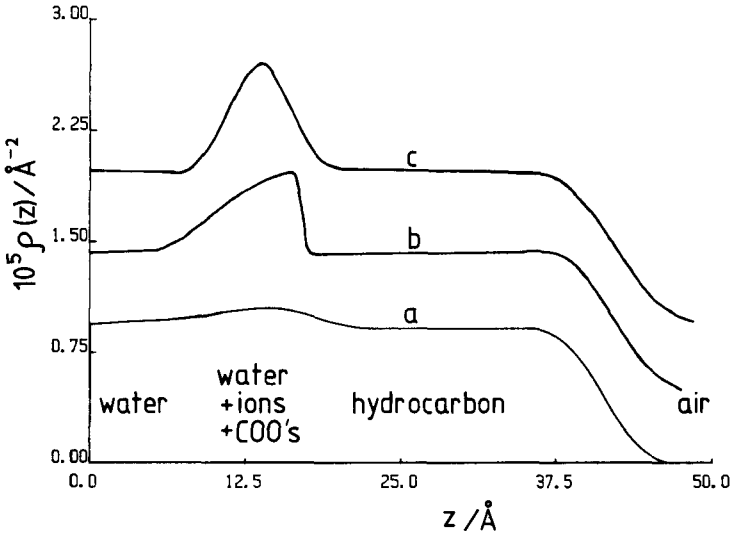

Figure 9. The scattering density profile, $\varrho(z)$, measured from an arbitrary origin in the water phase corresponding to some of the results in table 3. With cadmium ions in the subphase (*a*) corresponds to pH = 2·75 and (*b*) corresponds to pH = 6·5. Curve (*c*) corresponds to pH = 6·5 with lanthanum ions in the subphase.

unrealistic. For instance the thickness of the hydrocarbon layer became greater than the length of a model hydrocarbon chain (27·5 Å) if the thickness of the cadmium layer was fixed at less than 4 Å. If it was fixed at more than 12 Å the quality of fit deteriorated rapidly. We can therefore conclude that the thickness of the cadmium rich layer is 9 ± 3 Å. This confirms our initial interpretation that most of the surface excess of cadmium (or lanthanum) ions are in a layer within approximately 15 Å of the acid head groups. Fortunately, the correlation between the parameters d(Cd + COO) and ϱ(Cd + COO) meant that the excess scattering density Γ_{sd} (defined in equation (18)) turned out to be almost independent of the value at which d(Cd + COO) was fixed. The uncertainty in Γ_{sd} was estimated from the parameters obtained from fits with d(Cd + COO) fixed at these extreme values (i.e. 6 Å and 12 Å). Fixing the thickness of the cadmium rich layer at values between 6 Å and 12 Å caused the value for the thickness of the hydrocarbon layer, obtained by fitting to the data at a pH of 6·25, to vary from 26 Å to 23 Å. This is marginally less than the length of the fully extended hydrocarbon chain measured on a molecular model. This would suggest a tilt of the molecule of 25° ± 5° with respect to the layer normal, but it could also result from some contraction of the chain due to librations about the carbon–carbon bonds. We can conclude therefore that the molecules are not tilted by more than about 30° with respect to the surface normal at a pH of 6·25. The results in table 3 also indicate that there is a decrease in the thickness of the hydrocarbon layer as the pH is decreased which would suggest an increase in the tilt angle.

The parameter obtained by fitting to the data from a monolayer spread on $2{\cdot}5 \times 10^{-4}$ M lanthanum chloride suggest that the lanthanum ions are associated even more closely with the acid head groups than are the cadmium ions, since the thickness of the ion-rich layer is found to be 1·7 ± 0·3 Å while u(La + COO/water) is much the same as for cadmium.

5. Discussion

In this section we will show that the pH dependence of the layer containing the acid head groups and the counterion-rich subphase is consistent with a simple model. The model consists of a layer of carboxylate groups (perhaps containing some water molecules) with a mixture of water and couterions underneath it. The scattering density of this layer can be related to the number densities $N(z)$ of these three components and the number of electrons, a, associated with each component

$$\varrho(z) = r_e\{N_{cd}(z)\,a_{Cd^{++}} + N_{H_2O}(z)\,a_{H_2O} + N_{COO}(z)\,a_{COO}\}. \tag{14}$$

It is necessary to know the partial molecular volume of the acid head groups, water and cadmium counterions as a function of composition in order to eliminate the number density of water molecules in the counterion rich layer

$$\varrho(z) = r_e\left\{N_{Cd}(z)\left(a_{Cd^{++}} - a_{H_2O}\frac{v_{Cd^{++}}}{v_{H_2O}}\right) + N_{COO}(z)\left(a_{COO^-} - a_{H_2O}\frac{v_{COO}}{v_{H_2O}}\right) + \frac{a_{H_2O}}{v_{H_2O}}\right\}. \tag{15}$$

We assume that the molecular volumes are approximately independent of composition and take the value of v_{H_2O} as that of pure water. The molecular volume of cadmium, $v_{Cd^{++}}$, we assume to be zero since it is actually negative ($-30{\cdot}8\,cm^3\,mol^{-1}$) [12] in dilute solution. This assumption does not introduce any serious error since $a_{Cd^{++}} \gg a_{H_2O}$. The value of v_{COO} is less easy to estimate and so we shall treat $(a_{COO^-} - a_{H_2O}(v_{COO}/v_{H_2O}))$ as a parameter to be determined, but we would expect it to be between 5 and 15 electron units.

Integrating over the distance, z, perpendicular to the surface, and subtracting the term involving the scattering density of pure water from both sides gives

$$\int_{z=d_1}^{d_2}(\varrho(z) - \varrho_s)\,dz = r_e\{\Gamma_{Cd^{++}}a_{Cd^{++}} + \Gamma_{COO^-}a'\}, \tag{16}$$

where

$$a' = \left(a_{COO^-} - a_{H_2O}\frac{v_{COO}}{v_{H_2O}}\right), \tag{17}$$

and where Γ_x represents a surface excess of a molecule x (i.e. the number of molecules x per unit area of surface). The left-hand side of equation (16) is the excess scattering density, Γ_{sd}, in the head group and the counterion-rich layer and is related to the parameters derived from fitting the reflectivity data by

$$\Gamma_{sd} = \int_{d_1}^{d_2}(\varrho(z) - \varrho_s)\,dz = (\varrho(\mathrm{Cd + COO}) - \varrho(\mathrm{water}))\,\mathrm{d(Cd + COO)}. \tag{18}$$

We now propose a crude model to relate $\Gamma_{Cd^{++}}$ to the dissociation of the acid and the stability of the cadmium–acid complex. We ignore interactions between cadmium ions or protons when they are in the layer which we regard as being bound to the acid molecules; an equivalent assumption is made in deriving the Langmuir isotherm [13]. We then describe the equilibria

$$HA = H^+ + A^-$$
$$Cd^{++} + 2A^- = CdA_2$$

using equilibrium constants. The following expressions are equivalent to Langmuir isotherms ([13] equation (3)) with $n = 1$ and $n = 2$ respectively; similar approaches have been adopted by other authors (e.g. [15]),

$$K_a = \frac{\Gamma_{A^-}}{\Gamma_{HA}}[H^+], \tag{19}$$

$$K_s = \frac{\Gamma_{CA_2}}{\Gamma_{A^-}^2}\frac{1}{[Cd^{++}]}. \tag{20}$$

Assuming that the amount of ionized acid (Γ_{A^-}) not complexed with cadmium is negligible, then if a fraction α of the acid has been converted into the cadmium complex, we obtain:

$$[H^+] = K(\alpha^{-1/2} - \alpha^{1/2}), \tag{21}$$

where

$$K = (2K_a^2 K_s[Cd^{++}]\Gamma_0)^{1/2}, \tag{22}$$

and where Γ_0 is the total (complexed and not) surface excess of acid molecules. Solving this equation for α ($0 < \alpha < 1$) we find

$$\alpha = \left(\frac{\sqrt{([H^+]^2 + 4K^2)} - [H^+]}{2K}\right)^2. \tag{23}$$

If we assume that the surface excess of cadmium ions is a thin Stern layer (i.e. within approximately 15 Å of the head groups) and none in a diffuse layer extending further from the surface, then we can use $\Gamma_{Cd^{++}}$ as a measure of the degree of conversion of the acid into the cadmium complex,

$$\Gamma_{Cd^{++}} = \frac{\alpha}{2}\Gamma_0, \tag{24}$$

where the factor of 2 represents the ratio of the charge on the cadmium ion to that on an acid. Since $\Gamma_0 = \Gamma_{COO^-}$ we can now substitute equations (23) and (24) into equation (16)

$$\Gamma_{sd} = r_e\Gamma_0\left\{\frac{a_{Cd^{++}}}{2}\left(\frac{\sqrt{([H^+]^2 + 4K^2)} - [H^+]}{2K}\right)^2 + a'\right\}. \tag{25}$$

A plot of Γ_{sd} versus pH should give an S shape, as shown as points in figure 10. The line is a fit of equation (25) to the data with Γ_0, K and a' as adjustable parameters. The parameters which gave the best fit to the curve are as follows.

(i) $\Gamma_0 = 0{\cdot}046 \pm 0{\cdot}002\,\text{Å}^{-2}$ which corresponds to an area for an acid molecule $22 \pm 1\,\text{Å}^2$, in very good agreement with the value of 21 Å inferred from the surface pressure/surface area isotherm. This also confirms our supposition that all the surface excess of cadmium ions are within approximately 15 Å of the acid head groups and that the ionic species bound to the carboxylic acid group is Cd^{++} rather than $CdCl^+$ which has been suggested [14].

(ii) $pK = 5{\cdot}35 \pm 0{\cdot}05$, which is in good agreement with values deduced by other methods for the cadmium/carboxylic acid system. The ratio of cadmium stearate to stearic acid in deposited Langmuir–Blodgett films has been measured by electron spectroscopy for chemical analysis [15] and by neutron activation analysis [16]. Both

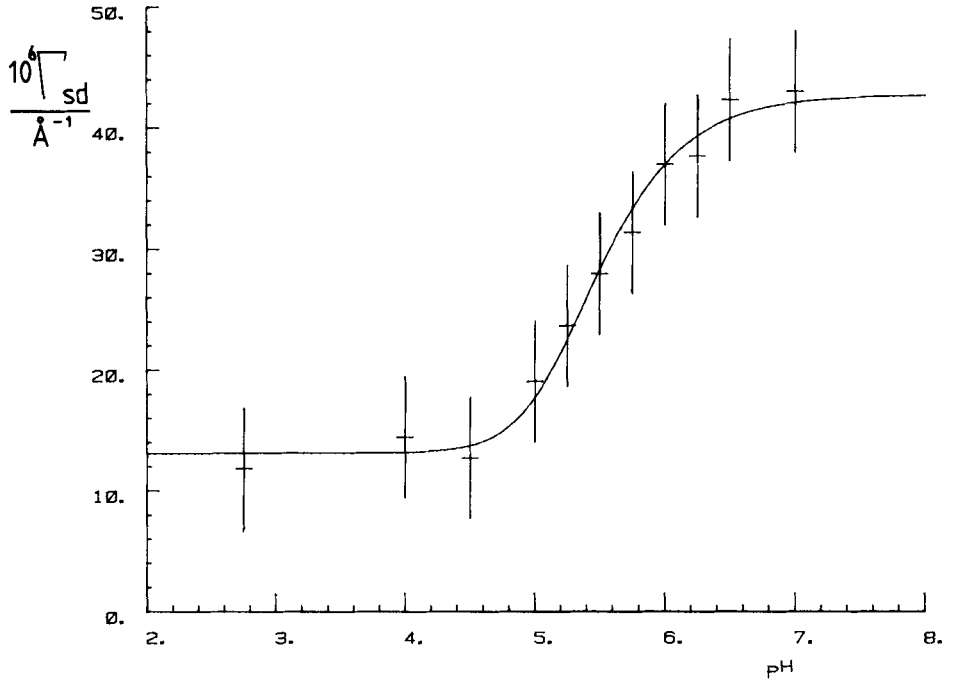

Figure 10. The excess scattering density, Γ_{sd}, as a function of pH for docosanoic acid on $2{\cdot}5 \times 10^{-6}$ M cadmium chloride solution.

techniques give a pH of about 5·5 for 50 per cent conversion of the acid to the soap. Equation (22) implies that K is a function of counterion type and concentration; this will be pursued in further work.

(iii) $a' = 10{\cdot}8 \pm 0{\cdot}9$, which is well within the range expected and equation (17) implies that a carboxylate group is about 40 per cent larger than a water molecule.

Although we have not studied the system containing lanthanum ions in the subphase as a function of pH, the data we have were obtained at a relatively high pH (6·5) and so we can assume $\alpha \approx 1$. Since the lanthanum ion has a charge of three electron units equation (25) with $\alpha = 1$ becomes

$$\Gamma_{sd} = r_e \Gamma_0 \left\{ \frac{a_{La^{+++}}}{3} + a' \right\}. \tag{26}$$

Using the value of a' obtained we can calculate that, for this system, $\Gamma_0 = 21 \pm 3$ Å. Again, this is in very good agreement with the value expected from the isotherm. It confirms that practically all the surface excess of lanthanum is in a layer close to the carboxylic acid head groups and that the binding species is La^{3+} rather than $LaCl^{++}$.

6. Conclusion

We have shown that X-ray reflectivity measurements on spread insoluble monolayers on an aqueous subphase can be made successfully using relatively simple apparatus. For docosanoic acid on a dilute solution of cadmium or lanthanum chloride, we have shown that virtually all the cations are within 15 Å of the acid head groups and that the hydrocarbon chains are within 30° of the surface normal (it

should be possible to measure the film thickness and hence the tilt angle much more precisely using neutron reflectivity from deuteriated docosanoic acid and experiments to do this are in progress). The effective pK for the binding of cadmium ions to the acid head groups is 5·35 ± 0·05.

Having established the X-ray reflectivity technique as a method for analysing the structure of thin films at a liquid/air interface we intend to use it to study the effects of changing the concentration and type of metal counterions in the subphase in order to test equation (22) and to establish the relative stability of different metal carboxylate complexes. The conformation of other insoluble surfactant molecules and polymers at the liquid surface will also be investigated. We believe the technique will find application in other fields where there is interest in the structure of a liquid/air interface.

The authors wish to thank Mr. M. R. Buhaenko (University of Bristol) and Dr. M. F. Daniel (Thornton Research Centre, Chester) for many useful and stimulating conversations. The Royal Signals and Radar Establishment, Malvern, are thanked for financial support.

Appendix

For an X-ray beam, partly polarized by prior reflection at a monochromator with take-off angle $2\theta_M$, it can be shown that the reflectivity at an ideally sharp interface with the same plane of incidence on the monochromator is given by a Fresnel type formula

$$R_F = \frac{\cos^2 2\theta_M |R_\parallel|^2 + |R_\perp|^2}{\cos^2 2\theta_M + 1}, \tag{A 1}$$

for $\mu \sin\theta_i < 1$, where

$$|R_\parallel|^2 = \frac{\tan^2(\theta_i - \theta_t)}{\tan^2(\theta_i + \theta_t)} \tag{A 2}$$

and

$$|R_\perp|^2 = \frac{\sin^2(\theta_i - \theta_t)}{\sin^2(\theta_i + \theta_t)} \tag{A 3}$$

and $R_F = 1$, for $\mu \sin\theta_i > 1$. Where θ_i, θ_t are the conventionally defined angles of incidence and transmission and μ is the refractive index.

References

[1] VINCENT, P. S., and ROBERTS, G. G., 1980, *Thin Solid Films*, **68**, 135.
[2] GAINES, G. L., 1966, *Insoluble Layers at Liquid–Gas Interfaces* (Interscience).
[3] ALS-NIELSEN, J., 1985, *Z. Phys.* B, **61**, 411.
[4] WEISS, A. H., DEUTSCH, M., BRASLAU, A., OCKO, B. M., and PERSHAN, P. S., 1986, *Rev. scient. Instrum.*, **57**, 2554.
[5] POMERANTZ, M., and SEGMULLER, A., 1980, *Thin Solid Films*, **68**, 33.
[6] HAYTER, J. B., HIGHFIELD, R. R., PALLMON, B. J., THOMAS, R. K., MCMULLEN, A. I., and PENFOLD, J., 1981, *J. chem. Soc. Faraday Trans. I*, **77**, 1437.
[7] BORN, M., and WOLF, E., 1970, *Principles of Optics*, Chap. 1 (Pergamon Press).
[8] CROWLEY, T. L., 1984, Thesis, University of Oxford, Chap. 7.
[9] BOWLER, R., HUGHES-DAVIES, T., ROSER, S. J., and THOMAS, R. K. (to be published).

[10] SPINK, J. A., and SANDERS, J. V., 1955, *Trans. Faraday Soc.*, **51**, 1154.
[11] *Harwell Subroutine Library Catalogue*, 1985, Report No. AERE R 9185, sixth edition.
[12] FRIEDMANN, H. L., and KRISHNAN, C. V., 1983, *Water, a Comprehensive Treatise*, edited by F. Franks (Plenum), p. 67.
[13] LANGMUIR, I., and SCHAEFER, V. J., 1937, *J. Am. chem. Soc.*, **59**, 2400.
[14] STEPHENS, J. F., 1972, *J. Colloid Interface Sci.*, **38**, 557.
[15] KOBAYASHI, K., and KYO TACKAOKA, 1986, *Bull. chem. Soc. Japan*, **59**, 933.
[16] PETROV, J. G., KULEFF, I., and PLATIKANOV, D. 1982, *J. Colloid Interface Sci.*, **88**, 29.